A Matrix Approach for the Evaluation of the Internal Impedance of Multilayered Cylindrical Structures

Article *in* Progress In Electromagnetics Research B · March 2011

DOI: 10.2528/PIERB11021505

CITATIONS
7

READS
44

1 author:

Jose A Brandao Faria
University of Lisbon
153 PUBLICATIONS **1,196** CITATIONS

SEE PROFILE

Progress In Electromagnetics Research B, Vol. 28, 351–367, 2011

A MATRIX APPROACH FOR THE EVALUATION OF THE INTERNAL IMPEDANCE OF MULTILAYERED CYLINDRICAL STRUCTURES

J. A. Brandão Faria

Instituto de Telecomunicações, Instituto Superior Técnico
Technical University of Lisbon
Av. Rovisco Pais, Lisboa 1049-001, Portugal

Abstract—A matrix technique for the computation of the per-unit-length internal impedance of radially inhomogeneous cylindrical structures is presented. The cylindrical structure is conceptually divided into a number of layers, each layer being characterized by its constitutive parameters, conductivity, permeability, and permittivity. Within this general framework, compound conductors, compound capacitors, compound magnetic cores, or any other compound structures resulting from a mix of the above, can be analyzed by using the very same tool. The developed software program, MLCS, which implements the mentioned matrix technique, also permits the evaluation of the electric and magnetic fields intensity at the layers' interfaces. The MLCS program is validated by using several application examples.

1. INTRODUCTION

Current advancements in material technology have opened up new horizons regarding the manufacturing of new devices and structures whose constitutive characteristics (conductivity, permeability and permittivity) can be tailored according to targeted specifications. In the case of circular cylindrical geometries this technological possibility leads, quite naturally, to multilayered structures, where, each layer can have predominant conducting properties, insulation properties, magnetic properties, or a mix of all.

The current interest paid to multilayered structures (in connection to its fabrication, and applications concerning superconductivity,

Received 15 February 2011, Accepted 18 March 2011, Scheduled 20 March 2011
Corresponding author: Prof. J. A. Brandão Faria (brandao.faria@ieee.org).

skin effect, eddy currents, and photonic metamaterial structures) is witnessed in recent publications [1–16]. Nonetheless, the research topic on multilayered radially inhomogeneous cylindrical structures has received scarce attention.

In this paper, we present a matrix formalism to deal with multilayered cylindrical structures which permits the frequency-domain evaluation of the structure's per-unit-length internal impedance, $\bar{Z}_{int} = R(\omega) + jX(\omega) = \bar{P}/I_{rms}^2$, where I_{rms} is the rms value of the current intensity flowing through the cylindrical structure's cross section, and $\bar{P}$ is the inward flux of the complex Poynting vector across the boundary cylindrical surface (of unit length), [17].

Figure 1 shows a longitudinal view of the circular cylindrical structure, driven by an enforced harmonic current i, which gives rise to longitudinal **A** and **E** vector fields, and azimuthal **H** and **B** vector fields. A cross section of the structure, showing its subdivision into N layers, is depicted in Fig. 2.

By taking into account the continuity of the tangential components of **E** and **H** vector fields at each interface, a transfer

Figure 1. Longitudinal view of the multilayered circular cylindrical structure.

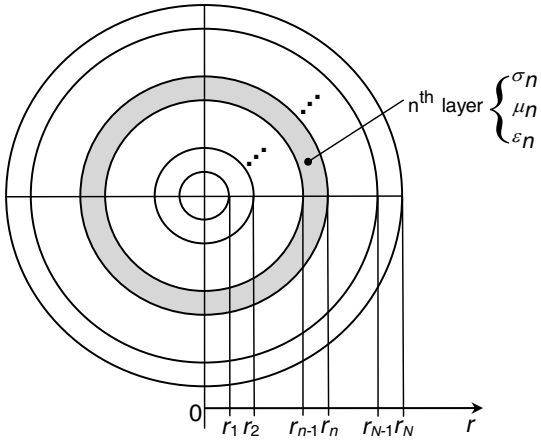

Figure 2. Cross section of the multilayered circular cylindrical structure.

matrix is defined for each layer. The matrix product of all transfer matrices allows the calculation of $\mathbf{E}$ and $\mathbf{H}$ at $r = r_N$, from where $\bar{Z}_{int}$ is determined.

We do not claim that our matrix approach is a novel one. In fact, similar treatments can be found in the analysis of stratified earth [18, 19], (in power line problems), and dielectric waveguides [20, 21], (in optical fiber problems). The added contribution of this work is that it encompasses radial variations of all the constitutive parameters of the structure (conductivity, permeability and permittivity). Within this general framework, compound conductors, compound capacitors, compound magnetic cores, or any other compound structures, can be analyzed by using the very same theoretical tool.

This paper is organized into seven sections, the first of which is introductory. Section 2 describes the fundamental frequency-domain equations for homogeneous cylindrical structures. In Sections 3 and 4, complex field phasors are determined at the layer's interfaces, including the inner cylinder. The per-unit-length internal impedance of the global structure is derived in Section 5. A series of computation examples, aimed at the validation of the software tool developed to implement the multilayer technique, are offered in Section 6. At last, Section 7 is devoted to conclusions.

2. FUNDAMENTAL EQUATIONS

For time harmonic regimes ($e^{j\omega t}$), the frequency-domain Maxwell curl equations read as [17],

$$\begin{cases} \nabla \times \bar{\mathbf{H}} = \bar{\mathbf{J}}_T = \bar{\mathbf{J}} + j\omega\bar{\mathbf{D}} = (\sigma + j\omega\varepsilon)\bar{\mathbf{E}} \\ \nabla \times \bar{\mathbf{E}} = -j\omega\bar{\mathbf{B}} = -j\omega\mu\bar{\mathbf{H}} \end{cases} \tag{1}$$

where σ, ε and μ respectively denote the conductivity, permittivity and magnetic permeability of the material medium. Overbar quantities in (1) represent complex amplitudes of field vectors.

In addition, from $\nabla \cdot \bar{\mathbf{B}} = 0$, it results $\bar{\mathbf{B}} = \nabla \times \bar{\mathbf{A}}$, where $\bar{\mathbf{A}}$ is the complex amplitude of the magnetic vector potential, with $\nabla \cdot \bar{\mathbf{A}} = 0$ (Coulomb gauge).

By combining the above results yields

$$\begin{cases} \nabla^2\bar{\mathbf{A}} + \bar{k}^2\bar{\mathbf{A}} = 0 \\ \bar{\mathbf{E}} = -j\omega\bar{\mathbf{A}} \\ \bar{\mathbf{H}} = \nabla \times \bar{\mathbf{A}}/\mu \end{cases} \tag{2}$$

where $\bar{k}$ is the complex wave number

$$\bar{k} = \sqrt{\omega^2\mu\varepsilon - j\omega\mu\sigma} \tag{3a}$$

When the material medium is a good conductor, displacement currents are negligibly small for frequencies up to the optical range, [17]. On the other hand, if the material medium is a lossless dielectric, then conduction currents are absent, that is

$$\bar{k} = \begin{cases} \sqrt{-j\omega\mu\sigma} \ : \text{ for a good conductor } \ (\mathbf{J}_T = \mathbf{J} = \sigma\mathbf{E}) \\ \omega\sqrt{\mu\varepsilon} \ : \text{ for a lossless dielectric } \ (\mathbf{J}_T = j\omega\varepsilon\mathbf{E}) \end{cases} \tag{3b}$$

For the case of an isolated system (proximity effects neglected) with longitudinal currents, where $\bar{\mathbf{A}} = \bar{A}(r)\,\vec{e}_z$, a cylindrical reference frame (r, θ, z) should be used.

In this case, the Laplacian equation in (2) yields

$$r^2 \frac{d^2\bar{A}}{dr^2} + r\frac{d\bar{A}}{dr} + \left(r\bar{k}\right)^2 \bar{A} = 0 \tag{4}$$

The general solution of (4) can be written as linear combination of Bessel, Neumann, or Hankel functions, that is, in compact notation, [22],

$$\bar{A}(x) = F f_0(x) + G g_0(x) \tag{5}$$

where $x = \bar{k}r$, F and G are complex constants to be determined with the help of boundary conditions, and

$$f_0(x) = J_0(x); \qquad g_0(x) = N_0(x) \tag{6a}$$

$$f_0(x) = H_0^{(1)}(x); \quad g_0(x) = H_0^{(2)}(x) \tag{6b}$$

In (6a), J_0 is the Bessel function of the first kind of order 0, and N_0 is the Neumann function of order 0. In (6b), $H_0^{(1)}$ and $H_0^{(2)}$ respectively denote the Hankel functions of first and second kinds of order 0.

From a numerical point of view (6a) should be employed for small values of $|x|$, whereas (6b) should be employed for large values of $|x|$.

The first derivatives of f_0 and g_0 satisfy, [23]

$$\frac{df_0}{dx} = -f_1 \quad \text{with} \quad f_1(x) = \begin{cases} J_1(x)\,, & \text{for small } |x| \\ H_1^{(1)}(x), & \text{for large } |x| \end{cases} \tag{7a}$$

$$\frac{dg_0}{dx} = -g_1 \quad \text{with} \quad g_1(x) = \begin{cases} N_1(x), & \text{for small } |x| \\ H_1^{(2)}(x), & \text{for large } |x| \end{cases} \tag{7b}$$

3. FIELD QUANTITIES AT LAYER INTERFACES

The cylindrical structure is made of N concentric layers (see Fig. 2). The generic nth layer is characterized by the following parameters: conductivity σ_n, permittivity ε_n, permeability μ_n, outer radius r_n, and inner radius r_{n-1} (for $n > 1$). The innermost region (region 1) is a cylinder of radius r_1.

For $r = r_n$, the electric field can be obtained from (2) as $\bar{E}_n = -j\omega\bar{A}(x_n)$, where $x_n = \bar{k}_n\, r_n$, where $\bar{k}_n$ is the wave number in (3) for the nth layer. The preceding result can be written in matrix form as

$$\bar{E}_n = \bar{E}(r_n) = -j\omega \left[\begin{array}{cc} f_0(x_n) & g_0(x_n) \end{array}\right] \left[\begin{array}{c} F_n \\ G_n \end{array}\right] \tag{8}$$

From $\bar{\mathbf{H}} = \bar{H}\,\vec{e}_\theta = \nabla \times \bar{\mathbf{A}}/\mu$, in (2), the magnetic field is obtained

$$\bar{H}(r) \;= -\frac{1}{\mu}\frac{d}{dr}\bar{A}(r) \;\;\rightarrow\;\; \bar{H}(r) = -\frac{\bar{k}}{\mu}\frac{d}{dx}\bar{A}(x) \tag{9}$$

For the nth layer, the magnetic field at the outer interface $r = r_n$ is determined using (9) and (7)

$$\bar{H}_n = \bar{H}(r_n) = \frac{\bar{k}_n}{\mu_n} \left[\begin{array}{cc} f_1(x_n) & g_1(x_n) \end{array}\right] \left[\begin{array}{c} F_n \\ G_n \end{array}\right] \tag{10}$$

Combining (8) and (10) yields

$$\left[\begin{array}{c} \bar{E}_n \\ \bar{H}_n \end{array}\right] = \left[\begin{array}{cc} -j\omega & 0 \\ 0 & \bar{k}_n/\mu_n \end{array}\right] \left[\begin{array}{cc} f_0(x_n) & g_0(x_n) \\ f_1(x_n) & g_1(x_n) \end{array}\right] \left[\begin{array}{c} F_n \\ G_n \end{array}\right] \tag{11}$$

The same process allows for the evaluation of the electric and magnetic field at the inner interface $r = r_{n-1}$ of layer n, that is

$$\left[\begin{array}{c} \bar{E}_{n-1} \\ \bar{H}_{n-1} \end{array}\right] = \left[\begin{array}{cc} -j\omega & 0 \\ 0 & \bar{k}_n/\mu_n \end{array}\right] \left[\begin{array}{cc} f_0(x'_n) & g_0(x'_n) \\ f_1(x'_n) & g_1(x'_n) \end{array}\right] \left[\begin{array}{c} F_n \\ G_n \end{array}\right] \tag{12}$$

where $x'_n = \bar{k}_n\, r_{n-1}$.

The F_n and G_n constants are determined by inverting (12)

$$\left[\begin{array}{c} F_n \\ G_n \end{array}\right] = \left[\begin{array}{cc} g_1(x'_n) & -g_0(x'_n) \\ -f_1(x'_n) & f_0(x'_n) \end{array}\right] \left[\begin{array}{cc} j/(\omega\Delta_n) & 0 \\ 0 & \mu_n/(\bar{k}_n\Delta_n) \end{array}\right] \left[\begin{array}{c} \bar{E}_{n-1} \\ \bar{H}_{n-1} \end{array}\right] \tag{13}$$

where Δ_n is the determinant of the second matrix on the right hand side of (12)

$$\Delta_n = f_0(x'_n)\; g_1(x'_n) \;-\; f_1(x'_n)\; g_0(x'_n) \tag{14}$$

At this stage it is important to remind a useful identity from Bessel functions theory [23],

$$\Delta = f_0(x)g_1(x) - f_1(x)g_0(x) = \begin{cases} \frac{-2}{\pi x}; \text{ when } f \equiv J \text{ and } g \equiv N \\ \frac{4j}{\pi x}; \text{ when } f \equiv H^{(1)} \text{ and } g \equiv H^{(2)} \end{cases} \tag{15}$$

Finally, by substituting (13) into (11), a relationship is established between the electric and magnetic fields observed at the two interfaces of the nth layer

$$\left[\begin{array}{c} \bar{E}_n \\ \bar{H}_n \end{array}\right] = \mathbf{T}_n \left[\begin{array}{c} \bar{E}_{n-1} \\ \bar{H}_{n-1} \end{array}\right]; \;\; \mathbf{T}_n = \left[\begin{array}{cc} a_n & b_n \\ c_n & d_n \end{array}\right] \tag{16}$$

Matrix $\mathbf{T}_n$ in (16) is the field transfer matrix for layer n ($n > 1$). The entries of matrix $\mathbf{T}_n$ are determined, from (11) and (12), through

$$\begin{bmatrix} a_n & b_n \\ c_n & d_n \end{bmatrix} = \begin{bmatrix} -j\omega & 0 \\ 0 & \bar{k}_n/\mu_n \end{bmatrix} \begin{bmatrix} f_0(x_n) & g_0(x_n) \\ f_1(x_n) & g_1(x_n) \end{bmatrix} \times \begin{bmatrix} g_1(x'_n) & -g_0(x'_n) \\ -f_1(x'_n) & f_0(x'_n) \end{bmatrix} \begin{bmatrix} j/(\omega\Delta_n) & 0 \\ 0 & \mu_n/(\bar{k}_n\Delta_n) \end{bmatrix} \quad (17)$$

yielding

$$a_n = \frac{1}{\Delta_n}\big(f_0(x_n)g_1(x'_n) - f_1(x'_n)g_0(x_n)\big) \quad (18)$$

$$b_n = \frac{\omega\mu_n}{j\bar{k}_n\Delta_n}\big(f_0(x'_n)g_0(x_n) - f_0(x_n)g_0(x'_n)\big) \quad (19)$$

$$c_n = \frac{j\bar{k}_n}{\omega\mu_n\Delta_n}\big(f_1(x_n)g_1(x'_n) - f_1(x'_n)g_1(x_n)\big) \quad (20)$$

$$d_n = \frac{1}{\Delta_n}\big(f_0(x'_n)g_1(x_n) - f_1(x_n)g_0(x'_n)\big) \quad (21)$$

The determinant of the field transfer matrix is given by

$$\det(\mathbf{T}_n) = a_n d_n - b_n c_n = \frac{f_0(x_n)g_1(x_n) - f_1(x_n)g_0(x_n)}{f_0(x'_n)g_1(x'_n) - f_1(x'_n)g_0(x'_n)} \quad (22)$$

Taking (15) into account, the result in (22) greatly simplifies

$$\det(\mathbf{T}_n) = \frac{x'_n}{x_n} = \frac{r_{n-1}}{r_n} \quad \text{for } n > 1 \quad (23)$$

4. INNER CYLINDER FIELD QUANTITIES

The region $0 < r < r_1$, (region 1), is a homogeneous cylinder where field vectors obey the boundary conditions $\bar{E}(r_1^-) = \bar{E}(r_1^+)$, $\bar{H}(r_1^-) = \bar{H}(r_1^+)$, and $\bar{H}(0) = 0$.

Using (16) yields

$$\begin{bmatrix} \bar{E}_1 \\ \bar{H}_1 \end{bmatrix} = \begin{bmatrix} a_1 & b_1 \\ c_1 & d_1 \end{bmatrix} \begin{bmatrix} \bar{E}(0) \\ 0 \end{bmatrix} \rightarrow \begin{cases} \bar{E}_1 = a_1\bar{E}(0) \\ \bar{H}_1 = c_1\bar{E}(0) \end{cases} \quad (24)$$

The surface impedance of the inner cylinder, measured at the interface $r = r_1$, is obtained from (24), (18), and (20), through

$$\bar{Z}_1 = \frac{\bar{E}_1}{\bar{H}_1} = \frac{a_1}{c_1} = \frac{\omega\mu_1 r_1}{jx_1}\,\frac{f_0(x_1)}{f_1(x_1)} \quad (25)$$

where $x_1 = \bar{k}_1 r_1$.

For a tubular system where region 1 is empty ($\mu_1 = \mu_0$, $\varepsilon_1 = \varepsilon_0$), the surface impedance $\bar{Z}_1$ is given by

$$\bar{Z}_1 = -j\sqrt{\frac{\mu_0}{\varepsilon_0}} \times \frac{f_0(\omega r_1/v_0)}{f_1(\omega r_1/v_0)} \tag{26}$$

where v_0 is the light speed in a vacuum, $v_0 = 1/\sqrt{\mu_0\varepsilon_0}$.

For low frequency regimes, that is, $\omega \ll v_0/r_1$, (26) leads to $\bar{Z}_1 \approx 2/(j\omega\varepsilon_0 r_1) \to \infty$.

For high frequency regimes, that is, $\omega \gg v_0/r_1$, (26) leads to $\bar{Z}_1 \approx -j\sqrt{\frac{\mu_0}{\varepsilon_0}} \cot\left(\frac{\omega r_1}{v_0} - \frac{\pi}{4}\right)$.

The preceding particular results for $\bar{Z}_1$, concerning a dielectric cylinder, were obtained by considering, respectively, Bessel function approximations for low arguments, and asymptotic expansions for large arguments [23].

5. ANALYSIS OF THE GLOBAL SYSTEM

By taking into account the continuity of the tangential field components at each interface, that is,

$$\bar{E}(r_n^-) = \bar{E}(r_n^+)\ ;\ \ \bar{H}(r_n^-) = \bar{H}(r_n^+) \quad \text{for } 1 \le n \le N$$

a relationship between the **E** and **H** fields at the most external ($r = r_N$) and most internal ($r = r_1$) layers of the inhomogeneous system can be obtained by successive multiplication of the transfer matrices pertaining to each layer

$$\begin{bmatrix} \bar{E}_N \\ \bar{H}_N \end{bmatrix} = \mathbf{T} \begin{bmatrix} \bar{E}_1 \\ \bar{H}_1 \end{bmatrix}\ ;\ \ \mathbf{T} = \mathbf{T}_N \cdots \mathbf{T}_n \cdots \mathbf{T}_2 = \begin{bmatrix} a & b \\ c & d \end{bmatrix} \tag{27}$$

The surface impedance $\bar{Z}_N$, measured at the external interface $r = r_N$, is determined through

$$\bar{E}_N = \bar{Z}_N \bar{H}_N; \quad \bar{Z}_N = \frac{a\bar{Z}_1 + b}{c\bar{Z}_1 + d} \tag{28}$$

where $\bar{Z}_1$ is defined in (25), (or in (26) for a tubular system).

The multilayered system carries an axial ($\vec{e}_z$) time-harmonic total current intensity $i(t) = \sqrt{2}\, I_{rms} \cos(\omega t + \alpha)$, which is characterized by its complex amplitude $\bar{I} = \sqrt{2}\, I_{rms}\, e^{j\alpha}$.

The application of the generalized Ampère law to a clockwise oriented circulation path **s** coinciding with the external circumference of radius r_N

$$\oint_{\mathbf{s}} \bar{\mathbf{H}} \cdot d\vec{s} = \int_{S_T} \bar{\mathbf{J}}_T \cdot \vec{n}_S\, dS \tag{29}$$

yields

$$2\pi r_N \bar{H}_N = \bar{I} \tag{30}$$

where S_T denotes the transverse cross section of the multilayered system (of radius r_N) and $\vec{n}_S = \vec{e}_z$ is the Stokes unit normal.

In order to determine the per-unit-length internal impedance $\bar{Z}_{int}(\Omega/\mathrm{m})$ of the multilayered system, the inward flux of the complex Poynting vector across the unit length cylindrical surface S of radius r_N is evaluated [17],

$$\bar{P} = \int\limits_S \left(\frac{\bar{\mathbf{E}} \times \bar{\mathbf{H}}^*}{2} \right) \cdot (-\vec{e}_r)\, dS \; = \frac{1}{2} \int\limits_S \left(\bar{E}_N \bar{H}_N^* \right) dS = \bar{Z}_{int}\, I_{rms}^2 \tag{31}$$

Taking (28), (30), and (31) into account the following final result is obtained

$$\bar{Z}_{int} = R + jX = \frac{\bar{Z}_N}{2\pi r_N} = \frac{1}{2\pi r_N} \times \frac{a\bar{Z}_1 + b}{c\bar{Z}_1 + d} \tag{32}$$

6. VALIDATION AND APPLICATION EXAMPLES

The set of Equations (3), (14), (18)–(21), (25), (27), (28), and (32) was translated into MATLAB code. The corresponding software program (MLCS), implementing the theoretical model of Multi-Layered Cylindrical Structures, needs validation.

The simplest way to validate our approach resorts to application examples of homogeneous structures whose per-unit-length internal impedance results have already been published (based on closed-form analytical formulas). The homogeneous structure is subdivided into N layers and then the multilayer treatment is applied. Comparison established between available direct results and those obtained by using MLCS will allow a performance evaluation of the latter. However, for a sound validation of MLCS an application example concerning an inhomogeneous structure is necessary. Unfortunately, in this respect, the literature is very scarce. Nonetheless, we will provide useful results steaming from a very recent development on the so-called Euler-Cauchy structures.

6.1. Homogeneous Structures

Two examples are analyzed here: a tubular conductor [24], and a disk capacitor [25].

6.1.1. Tubular Conductor

Per-unit-length internal impedance results, $\bar{Z}_{int}(\omega) = R(\omega) + j\omega L(\omega)$, concerning skin effect analysis for solid and tubular homogeneous conductors have been published in [24], where graphics of R/R_{dc} and L/L_{dc} against frequency were presented for a copper conductor of external radius $r_N = 4.72\,\text{mm}$, (note that R_{dc} and L_{dc} denote direct current values of R and L). The frequency range considered is 0 to 10 MHz. The structures considered are: (a) solid conductor, (b) tubular conductor with $r_1 = 0.4r_N$, (c) tubular conductor with $r_1 = 0.9r_N$.

We run MLCS for cases (a), (b), and (c), and obtained the results depicted in Fig. 3 and Fig. 4. The number of layers considered in the multilayer approach is $N = 50$, for all the cases.

Comparison established between MLCS results and those in Figs. 3, 4, 7, and 8 of [24] shows no apparent differences.

As mentioned above, Fig. 3 and Fig. 4 were obtained by subdividing the cylindrical structure into $N = 50$ layers. The remaining question is how the value assigned to N may affect the output of MLCS. From a theoretical point of view, since a homogeneous structure is being considered, N should have no effect on the final results. However, there might be a numerical problem. In fact, as the number of layers is increased the number of matrix operations (whose entries are combinations of Bessel functions) also increases, and consequently a degradation of numerical accuracy may occur. To check

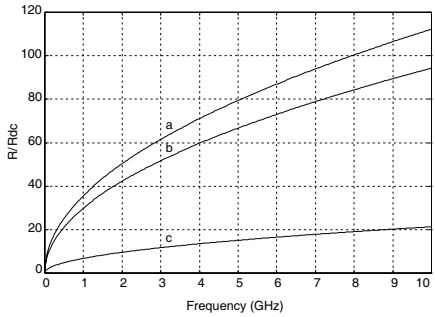

Figure 3. Plot of R/R_{dc} against frequency. (a) solid conductor; (b) tubular conductor where $r_1/r_N = 0.4$; (c) tubular conductor where $r_1/r_N = 0.9$. Compare with results in [24].

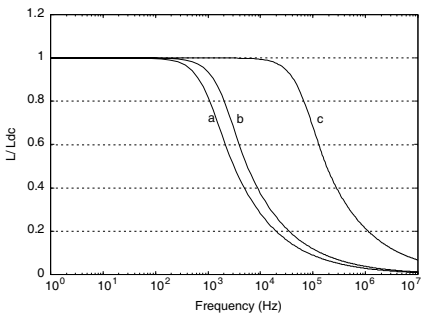

Figure 4. Plot of L/L_{dc} against frequency. (a) Solid conductor; (b) tubular conductor where $r_1/r_N = 0.4$; (c) tubular conductor where $r_1/r_N = 0.9$. Compare with results in [24].

on this problem we analyzed the solid cylinder case ($r_N = 4.72\,\text{mm}$), for $f = 10\,\text{MHz}$. The per-unit-length internal impedance was computed directly, through

$$\bar{Z}_{int} = R_{dc}\,\bar{k}r_N\,\frac{J_0(\bar{k}r_N)}{2J_1(\bar{k}r_N)} \tag{33}$$

and computed via MLCS, with N varying from 1 to 100.

Computation errors have been assessed, regarding the resistance and the reactance of the per-unit-length internal impedance, as follows

$$\begin{cases} R_{Error}(N) = \dfrac{\text{Re}\left\{\left(\bar{Z}_{int}(N)\right)_{MLCS} - \bar{Z}_{int}\right\}}{\left|\bar{Z}_{int}\right|} \\ X_{Error}(N) = \dfrac{\text{Im}\left\{\left(\bar{Z}_{int}(N)\right)_{MLCS} - \bar{Z}_{int}\right\}}{\left|\bar{Z}_{int}\right|} \end{cases} \tag{34}$$

The relative errors found, shown in Fig. 5, do not exceed 10^{-10}. Albeit negligibly small, the error functions plotted in Fig. 5, show a smooth evolution (near to zero) in the intervals $N \in [1,\ 25] \cup N \in [40,\ 60]$, and a series of spikes of random amplitude in the remaining range of N. This numerical noise is probably associated to some sort of instability in the calculation of the Bessel, Neumann, and Hankel functions, as has been suggested in [24].

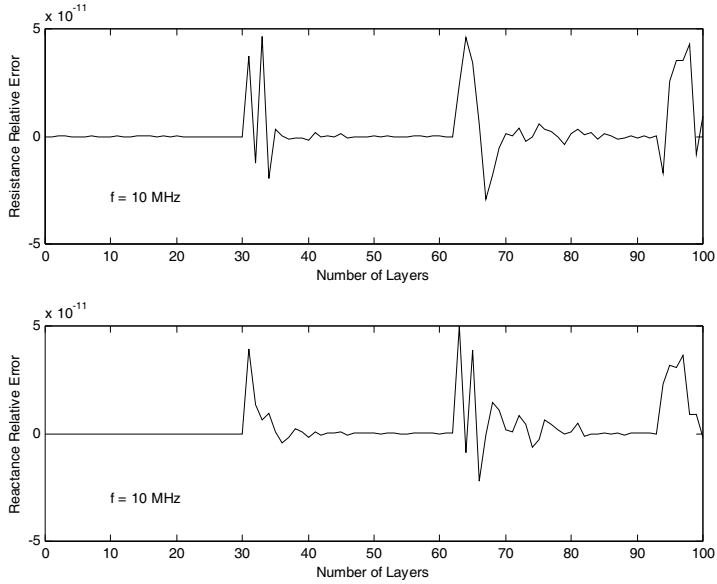

Figure 5. Resistance and reactance relative errors as a function of the number of layers. Results evaluated according (34), at 10 MHz.

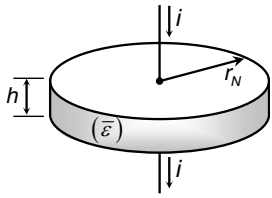

Figure 6. Disk capacitor structure.

6.1.2. Disk Capacitor

The structure depicted in Fig. 6 has been analyzed in [25]. A homogeneous lossy dielectric medium ($\varepsilon = 12\varepsilon_0$, loss angle $\delta = 0.012$) is sandwiched between two circular metallic discs of radius $r_N = 5\,\text{mm}$. The thickness of the dielectric material is $h = 50\mu\text{m} \ll r_N$.

In [25], the capacitor admittance $\bar{Y}(\omega)$ has been determined as a function of the frequency in the range 0 to 20 GHz. Graphical results for the conductance $G(\omega) = \text{Re}(\bar{Y})$ and for the susceptance $S(\omega) = \text{Im}(\bar{Y})$ are available in [25].

Using the problem data we run MLCS and obtained the per-unit-length internal impedance of the disk capacitor, $\left(\bar{Z}_{int}(\omega)\right)_{MLCS}$, and from it the corresponding admittance was evaluated

$$\left(\bar{Y}(\omega)\right)_{MLCS} = (G(\omega))_{MLCS} + j\,(S(\omega))_{MLCS} = \left(h \times \bar{Z}_{int}(\omega)\right)^{-1}_{MLCS} \quad (35)$$

The corresponding graphical results are shown in Fig. 7. As before, the number of layers considered in the multilayer approach is $N = 50$.

Comparison established between MLCS results and those in Fig. 4 of [25] shows no apparent differences.

It should be noted that although the results in this paper concern an axially undefined structure, they also apply to the finite length disk capacitor in Fig. 7. The reason is that the circular metallic disks are assumed to be perfect conductors, therefore ensuring that the electric field, perpendicular to the two disks, remains an axial field (for small h).

6.2. Euler-cauchy Inhomogeneous Structures

Considerer an inhomogeneous tubular conductor (displacement currents neglected, i.e., $\bar{k} = \sqrt{-j\omega\mu\sigma}$) where both the conductivity and permeability are functions of the radial coordinate, $\sigma = \sigma(r)$, $\mu = \mu(r)$, in the range $r_1 < r < r_N$.

For this situation the wave equation in (4) is no longer valid. It

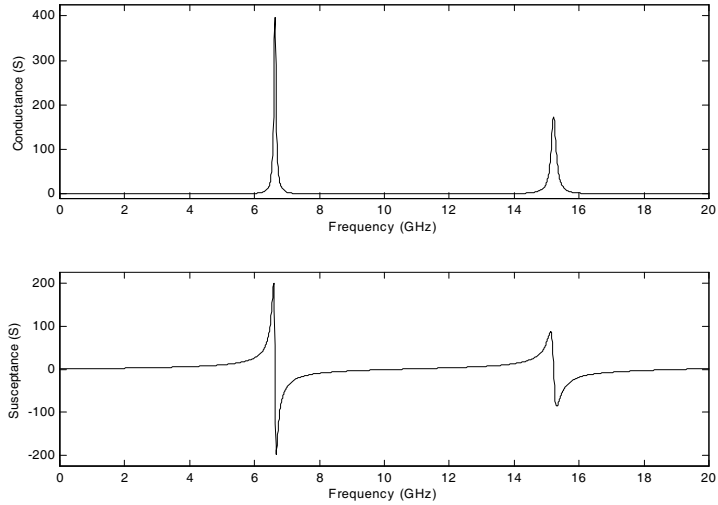

Figure 7. Disk capacitor conductance and susceptance against frequency. Compare with results in [25].

should be replaced by

$$r^2\frac{d^2\bar{A}}{dr^2}+\left(1-\frac{r}{\mu(r)}\frac{d\mu(r)}{dr}\right)r\frac{d\bar{A}}{dr}+\left(r\,\bar{k}(r)\right)^2\bar{A}=0 \tag{36}$$

where $\bar{k}^2(r)=-j\omega\sigma(r)\mu(r)$.

Equation (36) does not have, in general, a closed-form solution. However, if the functions $\sigma(r)$ and $\mu(r)$ are chosen such that

$$\mu(r)=\mu_1\left(\frac{r}{r_1}\right)^p \quad ; \quad \sigma(r)=\sigma_1\left(\frac{r_1}{r}\right)^{p+2} \tag{37}$$

we obtain from (36)

$$r^2\frac{d^2\bar{A}}{dr^2}+(1-p)\,r\frac{d\bar{A}}{dr}+\left(\bar{k}_1 r_1\right)^2\bar{A}=0 \tag{38}$$

where p is a real number, $\sigma_1=\sigma(r_1)$, $\mu_1=\mu(r_1)$, and $\bar{k}_1=\sqrt{-j\omega\mu_1\sigma_1}$.

The result in (38) describes the so-called homogeneous second order Euler-Cauchy equi-dimensional equation [26]. Cylindrical structures, whose constitutive medium is characterized by (37), are called Euler-Cauchy structures (ECS).

For $r_1 \le r \le r_N$, the solution of (38) can be written in closed form [26], as

$$\bar{A}(r)=A_1\,r^{m_1}+A_2\,r^{m_2} \tag{39}$$

where m_1 and m_2, given by

$$m_{1,2} = \frac{p}{2} \pm \sqrt{\left(\frac{p}{2}\right)^2 - \left(\bar{k}_1 r_1\right)^2} \tag{40}$$

are the roots of the characteristic equation: $m^2 - pm + (\bar{k}_1 r_1)^2 = 0$. The complex constants A_1 and A_2 in (39) are determined from the boundary conditions: $\bar{H}(r_1) = 0$; $\bar{H}(r_N) = \bar{I}/(2\pi r_N)$.

It can be proved that for arbitrary values of p, the general result for the per-unit-length internal impedance of the tubular conductor is given by

$$\bar{Z}_{int} = \frac{-j\omega\bar{A}(r_N)}{\bar{I}} = \frac{m_2(r_1/r_N)^{m_2} - m_1(r_1/r_N)^{m_1}}{2\pi\sigma_N r_N^2\left((r_1/r_N)^{m_1} - (r_1/r_N)^{m_2}\right)} \tag{41}$$

where $\sigma_N = \sigma(r_N) = \sigma_1(r_1/r_N)^{2+p}$.

As an application example we analyze here the case $p = -2$, where, from (37), $\sigma(r) = \sigma_N = \sigma_1$, $\mu(r) = \mu_1\,(r_1/r)^2$. For this case, the calculation of the per-unit-length internal impedance leads to

$$\bar{Z}_{int} = R(\omega) + jX(\omega) = \frac{1}{2\pi\sigma_1 r_N^2}\left(1 + u\left(\frac{1 + (r_1/r_N)^{2u}}{1 - (r_1/r_N)^{2u}}\right)\right) \tag{42}$$

where $u = u(\omega) = \sqrt{1 - (\bar{k}_1 r_1)^2}$.

For exemplification purposes consider the following data: $r_N = 3r_1 = 3\,\text{mm}$, $\sigma_1 = 5 \times 10^6\,\text{S/m}$, and $\mu_1 = 9\mu_0$ — see Fig. 8.

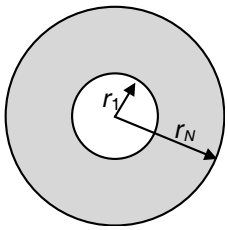

Figure 8. Cross section of an Euler-Cauchy tubular conductor where $\sigma(r) = 5 \times 10^6\,\text{S/m}$, $\mu(r) = \mu_0(3r_1/r)^2$, and $r_N = 3r_1 = 3\,\text{mm}$.

The direct computation of the per-unit-length internal impedance in (42) yields the solid lines $R(\omega)$ and $X(\omega)$ shown in Fig. 9, for a frequency sweep from 0 to 0.1 MHz.

Next, the multilayer technique was employed.

The tubular conductor was subdivided into 100 homogeneous layers of identical thickness, $\Delta r = (r_N - r_1)/(N - 1)$, each layer

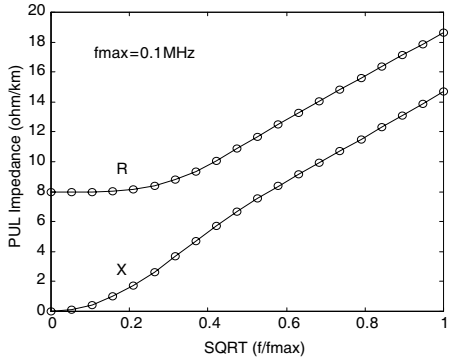

Figure 9. Real and imaginary parts of the per-unit-length internal impedance against frequency in the range 0 to 0.1 MHz. Solid lines are theoretical curves from (42). Circle marks are obtained from MLCS.

characterized by constant values of σ_n and μ_n

$$\sigma_n = \sigma_1; \quad \mu_n = \frac{1}{\Delta r} \int_{r_{n-1}}^{r_n} \mu(r) dr$$

Using the above parameter data we run MLCS and obtained the per-unit-length internal impedance of the ECS tubular conductor. Results obtained (identified by circle marks) are shown in Fig. 9, superposed to the theoretical curves. The agreement is almost perfect.

7. CONCLUSION

Inhomogeneous structures consisting of multilayered materials find application in a full range of areas, from microwaves to power systems. In this work, we paid special attention to radially inhomogeneous cylindrical structures, where the constitutive medium can be a conductor, a dielectric, a magnetic material, or a mix of all of them.

The supporting theory for the analysis of multilayered cylinders was developed by making use of a matrix approach, where each layer is characterized by its own field transfer matrix; the inhomogeneous structure being described by a global transfer matrix (i.e., the matrix product of all the individual layer transfer matrices). The presented approach permits not only the evaluation of the per-unit-length internal impedance of the cylindrical structure, but also the evaluation of the E and H fields at the layers' interfaces.

The theoretical results were translated into a software program, MLCS, whose main output is the frequency-dependent cylinder's internal impedance. MLCS was validated with the help of several application examples taken from the literature, and also by considering the special case of an Euler-Cauchy structure.

REFERENCES

1. Matrone, A., S. Ferraiuolo, and L. Martini, "Development of low-losses current leads based on multilayered Bi223/Ag conductors," *Il Nuovo Cimento D*, Vol. 19, No. 8–9, 1469–1475, 1997.
2. Olsen, S., C. Traeholt, A. Kuhle, O. Tonnesen, M. Daumling, and J. Oestergaard, "Loss and inductance investigations in a 4-layer superconducting prototype cable conductor," *IEEE Trans. Appl. Supercond.*, Vol. 9, No. 2, 833–836, 1999.
3. Martini, L., F. Barberis, R. Bert, G. Volpini, L. Bigoni, and F. Curcio, "AFM multilayered Bi-2223 conductors for 13 kA current leads for CERN," *Physica C: Superconductivity*, Vol. 341–348, Part 4, 2513–2516, 2000.
4. Tsuda, M., A. Alamgir, Y. Ito, T. Harano, N. Harada, T. Hamajima, M. Ono, and H. Takano, "Influence of current distribution on conductor performance in coaxial multi-layer HTS conductor," *IEEE Trans. Appl. Supercond.*, Vol. 12, No. 1, 1643–1646, 2002.
5. Jobava, R., R. Heinrich, D. Pommerenke, W. Kalkner, and A. Gheonjian, "Efficient FDTD simulation of fields in coaxial cables with multi-layered insulation partially formed by dispersive layers of extremely high permittivity," *Proc. Direct and Inv. Probl. of Elelectromag. and Accoustic Wave Theory 2002*, 91–94, Tbilisi, Georgia, 2002.
6. Honjo, S., N. Hobara, Y. Takahashi, H. Hashimoto, K. Narita, and T. Yamada, "Efficient finite element analysis of electromagnetic properties in multi-layer superconducting power cables," *IEEE Trans. Appl. Supercond.*, Vol. 13, No. 2, 1894–1897, 2003.
7. Maher, E., J. Abell, R. Chakalova, Y. Cheung, T. Button, and P. Tixador, "Multi-layer coated conductor cylinders: An alternative approach to superconducting coil fabrication," *Supercond. Sci. Technol.*, Vol. 17, No. 12, 1440–1445, 2004.
8. Tang, X., H. Zhang, H. Su, Y. Shi, and X. Jiang, "Characteristics of thin film inductors using magnetic multilayered films with ceramic intermediate layers," *J. Magnetism and Magn. Materials*, Vol. 294, No. 1, 29–52, 2005.

9. Jiang, Z., N. Amemiya, and M. Nakahata, "Numerical calculation of AC losses in multi-layer superconducting cables composed of coated conductors," *Supercond. Sci. Technol.*, Vol. 21, No. 2, 025013, 2008.
10. Zhuang, Y., B. Rejaei, H. Schellevis, M. Vroubel, and J. Burghartz, "Magnetic-multilayered interconnects featuring skin effect suppression," *IEEE Electron. Dev. Lett.*, Vol. 29, No. 4, 319–321, 2008.
11. Lesniewska, E. and R. Rajchert, "Application of the field-circuit method for the computation of measurement properties of current transformers with cores consisting of different magnetic materials," *IEEE Trans. Magn.*, Vol. 46, No. 10, 3778–3783, 2010.
12. Chong, Y., D. Gorlitz, S. Martens, M. Yau, S. Allende, J. Bachmann, and K. Nielsch, "Multilayered core/shell nanowires displaying two distinct magnetic swtching events," *Adv. Materials.*, Vol. 22, No. 22, 2435–2439, 2010.
13. Tellini, B. and M. Bologna, "Magnetic composite materials and arbitrary B-H relationships," *IEEE Trans. Magn.*, Vol. 46, No. 12, 3967–3972, 2010.
14. Entezar, S., A. Nambar, H. Rahini, and H. Tajalli, "Localized waves at the surface of a single-negative periodic multilayer structure," *Journal of Electromagnetic Waves and Applications*, Vol. 23, 171–182, 2009.
15. Oraizi, H. and M. Afsahi, "Transmission line modelling and numerical simulation for the analysis and optimum design of metamaterial multilayer structures," *Progress In Electromgnetics Research B*, Vol. 14, 263–283, 2009.
16. Golmohammadi, S., Y. Rouhani, K. Abbasian, and A. Rostami, "Photonic bandgaps in quasiperiodic multilayer structures using Fourier transform of the refractive index profile," *Progress In Electromgnetics Research B*, Vol. 18, 311–325, 2009.
17. Faria, J., *Electromagnetic Foundations of Electrical Engineering*, Wiley, Chichester, UK, 2008.
18. Ametani, A., "Stratified earth effects on wave propagation: Frequency-dependent parameters," *IEEE Trans. Power App. Syst.*, Vol. 93, No. 5, 1223–1239, 1974.
19. Deri, A., G. Tevan, A. Semlyen, and A. Castanheira, "The complex ground return plane: A simplified model for homogeneous and multi-layer earth return," *IEEE Trans. Power App. Syst.*, Vol. 100, No. 8, 3686–3693, 1981.
20. Neves, M. and J. Faria, "An efficient method for analyzing graded-

index optical fibers," *Microwave and Opt. Tech. Letters*, Vol. 6, No. 7, 426–431, 1993.

21. Neves, M. and J. Faria, "On the discretization process involved in the staircase approximation technique for analyzing radially inhomogeneous optical fibers," *Microwave and Opt. Tech. Letters*, Vol. 6, No. 12, 710–715, 1993.
22. Simonyi, K., *Foundations of Electrical Engineering*, Pergamon Press, Oxford, UK, 1963.
23. Watson, G., *A Treatise on the Theory of Bessel Functions*, Cambridge University Press, Cambridge, UK, 1992.
24. Vujevic, S., V. Boras, and P. Sarajcev, "A novel algorithm for internal impedance computation of solid and tubular cylindrical conductors," *Int. Rev. Electrical Eng.*, Vol. 4, No. 6, 1418–1425, 2009.
25. Faria, J., "Electromagnetic field approach to the modeling of disk-capacitor devices," *Microwave and Opt. Tech. Letters*, Vol. 48, No. 8, 1467–1472, 2006.
26. Wylie, C., *Advanced Engineering Mathematics*, Mc-Graw-Hill, New York, USA, 1975.